NATIONAL ADVISORY COMMITTEE FOR AERONAUTICS

TECHNICAL NOTE 3242

PRELIMINARY RESULTS FROM FLOW-FIELD MEASUREMENTS AROUND SINGLE AND TANDEM ROTORS IN THE LANGLEY FULL-SCALE TUNNEL

By Harry H. Heyson

Langley Aeronautical Laboratory
Langley Field, Va.

Washington
November 1954

NATIONAL ADVISORY COMMITTEE FOR AERONAUTICS

TECHNICAL NOTE 3242

PRELIMINARY RESULTS FROM FLOW-FIELD MEASUREMENTS AROUND SINGLE AND TANDEM ROTORS IN THE LANGLEY FULL-SCALE TUNNEL

By Harry H. Heyson

SUMMARY

An investigation of the flow field behind a single rotor and a tandem rotor has been conducted in the Langley full-scale tunnel at a tip-speed ratio of 0.15. A chart of the flow angles and dynamic-pressure contours behind the single rotor is presented. Measurements of the vertical induced velocity around the single rotor are presented and compared with those of theory. The induced velocity in the plane of the single rotor, as obtained by fairing the survey data, and the downwash angles near the tandem rotor are also compared with those of theory.

The comparisons indicate that theory is sufficiently accurate for use in preliminary design calculations and that the flow behind a rotor is very much like the flow behind a wing.

INTRODUCTION

A review of available rotary-wing flow-field knowledge (ref. 1) has indicated a scarcity of information on the forward-flight regimes of operation. Consequently, in 1953 the staff of the Langley full-scale tunnel undertook a small exploratory investigation of the flow around single and tandem rotors. By using the experience gained in this series of tests, a fairly complete test program of the single-rotor configuration, with a wide range of variables, was planned and was finally completed about April 1954. Only a portion of the data obtained in the more recent surveys has been reduced at the present time and the portion which is presented here should be considered preliminary. Only one tip-speed ratio is discussed, but the data should be applicable to most present-day helicopters at speeds near cruising.

SYMBOLS

C_L	rotor lift coefficient, $\text{Lift}/q_o \pi R^2$
q	local dynamic pressure, lb/sq ft
q_o	free-stream dynamic pressure, lb/sq ft
R	rotor radius, ft
v	local vertical induced velocity, ft/sec
v_o	theoretical vertical induced velocity at center of rotor, ft/sec
Z	vertical height above tip-path plane of rotor, ft
ϵ	local downwash angle, deg
ϵ_o	theoretical downwash angle at center of single rotor, deg
μ	rotor tip-speed ratio
χ	wake skew angle, angle between axis of wake and axis of tip-path plane, deg

APPARATUS

The experimental apparatus used in the single-rotor tests is shown in figure 1 and the arrangement used in the tandem-rotor tests is shown in figure 2.

The rotors used were of the teetering or seesaw type and had rectangular, untwisted blades of NACA 0012 airfoil section. The rotor radius was $7\frac{1}{2}$ feet and the rotor solidity was 0.0543. The rotor tip speed was 500 ft/sec.

A five-tube survey rake was used throughout the tests to measure stream pitch and yaw angles and dynamic pressures. This rake is fully described in reference 2.

CORRECTIONS

A reflection plane was used in all the tests, and for this configuration the Langley full-scale tunnel has no appreciable jet-boundary correction (ref. 3).

In order to correct for the flow about the supporting mechanism and for airstream misalinement, data were taken twice at each point in space - once with and once without the rotor blades installed. The difference is considered to be characteristic of the isolated rotor.

The rake used is incapable of measuring instantaneous variations of flow angles and velocities such as might be desired for a complete vibration analysis. Therefore, all data are time-averaged values.

RESULTS AND DISCUSSION

The lines in figure 3 show the extent of the survey planes in the single-rotor tests. All the survey planes are perpendicular to the longitudinal center line of the tunnel. They are located at the leading edge of the rotor disk, one-fourth of the way back, at the center, three-fourths of the way back, and 7 percent of a radius behind the trailing edge of the rotor disk. Two additional planes farther rearward were also surveyed, but the results are not yet available.

Figure 4 maps the flow 7 percent of a radius behind the trailing edge. Figure 4(a) shows the angular variations in the flow. The vectors represent the deviation of the flow, in degrees, from a path parallel to the tunnel center line. The vertical component of the vector is the downwash angle; the lateral component is the sidewash angle. The general effect given by the figure is much like that given by a tuft-grid photograph. Notice the striking similarity to the flow behind a lifting wing. The sharp change in sidewash angle just below the level of the rotor indicates that the trailing vortex sheet is located in that region. The strength of vorticity in the sheet increases from the center to the tips of the rotor. The beginning of the rolling up of the sheet into the large tip vortices which are almost directly behind the outboard edges of the rotor disk may be seen. Because of the different blade loading on each side of the disk, there is a slight asymmetry in the flow in this survey plane. For example, the stronger tip vortex (behind the advancing side) has moved a little more toward the center of the rotor than has the weaker vortex (behind the retreating side).

Figure 4(b) shows the variation of local dynamic pressure in the same survey plane. It is evident that large velocity changes are confined to a relatively small area behind the rotor. The dynamic pressure

in this area is greater than that of the free stream since the rotor, in helicopter operation, is adding energy to the airstream. The unusual humped shape of the pressure curves in the center of the chart is due to the forward tilt of the rotor. The center part, which is high, has just come off the raised trailing edge of the disk; the outer region, which is lower, comes from the lower outboard edges of the disk. Although it is not seen in figure 4(b), the velocities well below the rotor are slightly less than free stream, whereas those above the rotor are slightly greater. This effect is very much like that created by the circulation around a lifting wing.

Figure 5 shows the induced vertical velocity in the five survey planes. The ordinate is the vertical height, in terms of the radius, above the rotor. The tip-path plane of the rotor is represented by $Z/R = 0$. The abscissa is the vertical induced velocity divided by the theoretical downwash velocity at the center of the rotor. The experimental points (circles) represent the average induced velocity across the disk. The theoretical values for the longitudinal center line, as calculated by Castles and De Leeuw (ref. 4), are shown as a solid line.

By comparing the two sets of values on this basis, it may be seen that the theory underestimates the induced velocity above the rotor. The agreement below the rotor is good in the three middle survey planes. At the leading edge of the rotor, the vertical extent of the upwash region is smaller than that predicted by theory. Near the trailing edge of the rotor, where the theory indicates a constant downwash of v/v_o equal to slightly more than 2, the experimental points indicate that the downwash continues to build up across the wake and reaches a maximum value of about 3.

A knowledge of the induced velocity in the plane of the rotor itself is very useful in accurate performance and stability calculations. In order to get this information, lines were faired through the measured points of figure 5 and the values at the rotor disk were picked off. These values were compared with the theoretical values for the longitudinal center line of the rotor disk, and the comparison is shown in figure 6. The solid line represents the values computed in reference 4. No correction has been applied to the theory for the effect of lateral asymmetry of the blade-bound vortex system. This effect tends to reduce the slope slightly, but it can be shown to be small and within the order of accuracy of the measurements. (See the appendix.) An additional error is introduced by the presentation of the measured results as averages across the disk. Since a radial distribution of load on the rotor is known to exist, the average values are higher than the single values in the longitudinal plane of symmetry. This error is greatest in the center of the rotor and disappears at the leading and trailing edges. Its maximum magnitude may be estimated from the difference between the value of v/v_o and 1.0 at the center of the rotor.

In general, the data of figures 5 and 6 indicate that the theory of reference 4 is sufficiently accurate that it may, with certain reservations, be used to calculate the induced flow or the downwash angles to a sufficient degree of accuracy to be adequate for initial design considerations.

The results of the short exploratory investigation of the tandem-rotor system are now discussed. These surveys covered the planes shown in figure 7. The survey planes were at the center line of the front rotor, the leading edge of the rear rotor, the center line of the rear rotor, and 7 percent of a radius behind the trailing edge of the rear rotor. The two rotors were at equal heights above the center line of the test machine; that is, there was no vertical offset. The gap between the rotors was very small - about 7 percent of a radius.

Before examining the data of the Langley full-scale tunnel, first look at a tuft-grid photograph taken behind a tandem-rotor model in the Langley stability tunnel (fig. 8). Despite the addition of a second rotor, there is still only one set of trailing tip vortices. Although distorted (note the vertical elongation of the vortex behind the right or retreating side of the rear rotor), the flow is still essentially the same as that behind a single rotor. Similar photographs, taken under a wide variety of operating conditions, indicate that this observation remains valid until either very high fuselage attitudes or very high lift coefficients are reached. For the surveys of the Langley full-scale tunnel that are shown in the subsequent figures, the fuselage attitude and lift coefficient are both much lower than for this case. It would, therefore, be expected that the data would show the effect of a single pair of tip vortices.

Figure 9 shows the downwash angles, averaged across the span, as measured in the surveys. It should be noted, before examining the figures in detail, that the points indicate only the downwash angle - not downwash velocity. The points have been divided by the theoretical downwash angle at the center of the rotor. Also, in these charts $Z/R = 0$ represents the tip-path plane of the front rotor. For this condition, however, the rotors were trimmed in such a manner that both tip-path planes are nearly coincident, and $Z/R = 0$ may, therefore, be considered to represent the tip-path plane of either rotor. The solid line represents the theoretical variation of downwash angle for a single rotor. In the initial portion of these tests, the rear-rotor blades were removed and the front rotor was set to a given flight condition. This configuration was then surveyed as a single rotor. The results are shown in figure 9 as circles. It is evident from these points that, if the theory is used to predict only the downwash angles rather than the total induced velocity, it is considerably more accurate. The error is largest in the more rearward planes.

The rear rotor was then placed on the helicopter, and the overall tandem configuration was then set to operate at the same values of lift coefficient and useful drag-lift ratio as in the single-rotor portion of the test. In setting this condition, only the rear-rotor controls were used. The tandem rotor was then surveyed at the same points in space as the single rotor. The resultant values are plotted as squares in figure 9.

The addition of the rear rotor affects the front rotor by adding a small, but significant, upwash component to the flow in the forward survey planes. Since the front-rotor control setting remained unchanged, this upwash must increase the blade angles of attack of the front rotor and, consequently, the portion of the total lift and drag that it carries. Thus, the tandem-rotor model is equivalent to a flight article having its center of gravity somewhat forward of the midpoint between the rotors.

Also evident in the vicinity of the rear rotor is that the additional downward impulse imparted to the air flow by adding a second rotor resulted in very large increases in the downwash angles. In each location, however, the general shape of the downwash curves, except for magnitude, is still the same. This effect is to be expected from the general flow pattern.

Figure 10 compares the downwash at the plane of each rotor as faired from the previous figures. The rear rotor is seen to operate in a total downwash field approximately three times as great as that of the front rotor. Therefore, it might be expected that the rear rotor would require about three times as much induced power as the front rotor. Power measurements indicate that this condition is actually true. (See ref. 5.)

Figure 9 indicates that the induced power requirement of the rear rotor is a function of its height relative to the front rotor. Different configurations or different combinations of control may result in large changes in the induced power requirement.

Figures 9 and 10 indicate that a knowledge of the flow field in and around the rotors is sufficient for explaining and estimating the size of the induced losses in tandem-rotor configurations.

CONCLUSIONS

Preliminary results from flow-field measurements around single and tandem rotors in the Langley full-scale tunnel indicate the following conclusions:

1. The time-averaged flow field caused by a rotor in normal helicopter attitudes is very much like that of a wing.

2. The time-averaged downstream flow field generated by a lightly loaded, clean, tandem-rotor helicopter is much like that generated by a single-rotor helicopter.

3. The present surveys indicate that the induced losses in tandem-rotor helicopter configurations may be explained and their approximate magnitude estimated if a sufficient knowledge of their flow field is available.

4. The theoretical flow fields about a rotor, as calculated in NACA TN 2912, may, with certain reservations, be used to calculate the induced flow or the downwash angles to a sufficient degree of accuracy to be adequate for initial design considerations.

Langley Aeronautical Laboratory,
National Advisory Committee for Aeronautics,
Langley Field, Va., June 18, 1954.

APPENDIX

APPROXIMATE CALCULATION OF VERTICAL INDUCED VELOCITY DUE TO ASYMMETRY OF BLADE-BOUND VORTICES

Equation (10) of reference 6 gives the additional vertical induced velocity (at the 75-percent-radius station) due to an asymmetrical blade-bound vortex system as

$$\Delta v = -0.6 \frac{\Gamma_1 b}{2\pi R} \cos \psi \tag{1}$$

Equation (5) of reference 6 gives

$$\Gamma_1 = \frac{3}{2} \mu \Gamma_o \tag{2}$$

and

$$\Gamma_o = \frac{2W}{b\rho R(\Omega R)\left(1 - \frac{3}{2}\mu^2\right)} \tag{3}$$

where the symbols are defined as follows:

b	number of blades in rotor
W	gross weight of helicopter, lb
Γ	circulation, $\Gamma_o - \Gamma_1 \sin \psi$, ft^3/sec
Γ_o	constant portion of blade-bound circulation
Γ_1	sinusoidal variation of blade-bound circulation
ρ	mass density of air, $slugs/ft^3$
ψ	blade azimuth angle measured from downwind position in direction of rotation, radians
Ω	rotor rotational speed, radians/sec

Since $q_o = \frac{\rho}{2}\mu^2(\Omega R)^2$ and $C_L = \frac{\text{Lift}}{q_o \pi R^2}$, the following equation can be derived:

$$W = \text{Lift} = C_L \frac{\rho}{2}\mu^2(\Omega R)^2\pi R^2 \tag{4}$$

Substitution of equations (3) and (4) into equation (2) yields

$$\Gamma_1 = \frac{3}{2}\frac{\mu^3 C_L(\Omega R)\pi R^2}{bR\left(1 - \frac{3}{2}\mu^2\right)} \tag{5}$$

and equation (1) becomes

$$\Delta v = -\frac{1.8}{4}\frac{\mu^3 C_L(\Omega R)}{\left(1 - \frac{3}{2}\mu^2\right)}\cos\psi \tag{6}$$

The downwash angle at the center of a uniformly loaded rotor to a first approximation is

$$\epsilon_o = \frac{C_L}{4} \tag{7}$$

and the corresponding vertical induced velocity is

$$v_o \approx \mu(\Omega R)\epsilon = \frac{\mu(\Omega R)C_L}{4} \tag{8}$$

Finally, dividing equation (6) by equation (8) gives

$$\frac{\Delta v}{v_o} = -1.8\frac{\mu^2}{1 - \frac{3}{2}\mu^2}\cos\psi \tag{9}$$

At a tip-speed ratio of 0.15, equation (9) shows that $\Delta v/v_o$ is only -0.042 at the 75 percent radius and $\psi = 0$. This effect is within the accuracy of the measured data points presented in this paper.

REFERENCES

1. Gessow, Alfred: Review of Information on Induced Flow of a Lifting Rotor. NACA TN 3238, 1954.

2. Lange, Roy H., and Fink, Marvin P.: Studies of the Flow Field Behind a Large-Scale 47.5° Sweptback Wing Having Circular-Arc Airfoil Sections and Equipped With Drooped-Nose and Plain Flaps. NACA RM L51L12, 1952.

3. Silverstein, Abe, and Katzoff, S.: Experimental Investigation of Wind-Tunnel Interference on the Downwash Behind an Airfoil. NACA Rep. 609, 1937.

4. Castles, Walter, Jr., and De Leeuw, Jacob Henri: The Normal Component of the Induced Velocity in the Vicinity of a Lifting Rotor and Some Examples of Its Application. NACA TN 2912, 1953.

5. Dingeldein, Richard C.: Wind-Tunnel Studies of the Performance of Multirotor Configurations. NACA TN 3236, 1954.

6. Drees, J. Meijer: A Theory of Airflow Through Rotors and Its Application to Some Helicopter Problems. Jour. Helicopter Assoc. of Great Britain, vol. 3, no. 2, July-Aug.-Sept. 1949, pp. 79-104.

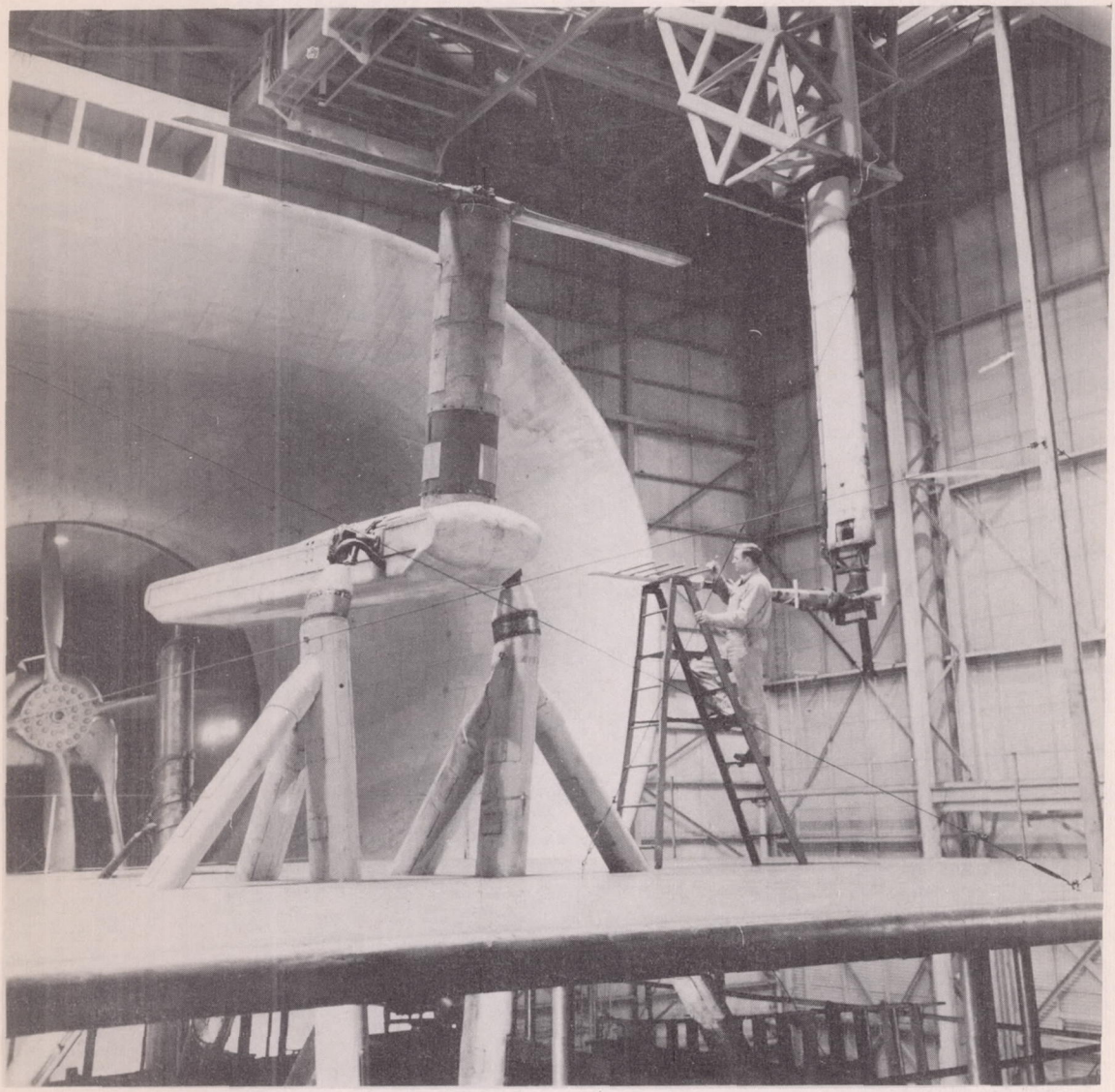

L-83265

Figure 1.- Single-rotor apparatus mounted in the Langley full-scale tunnel.

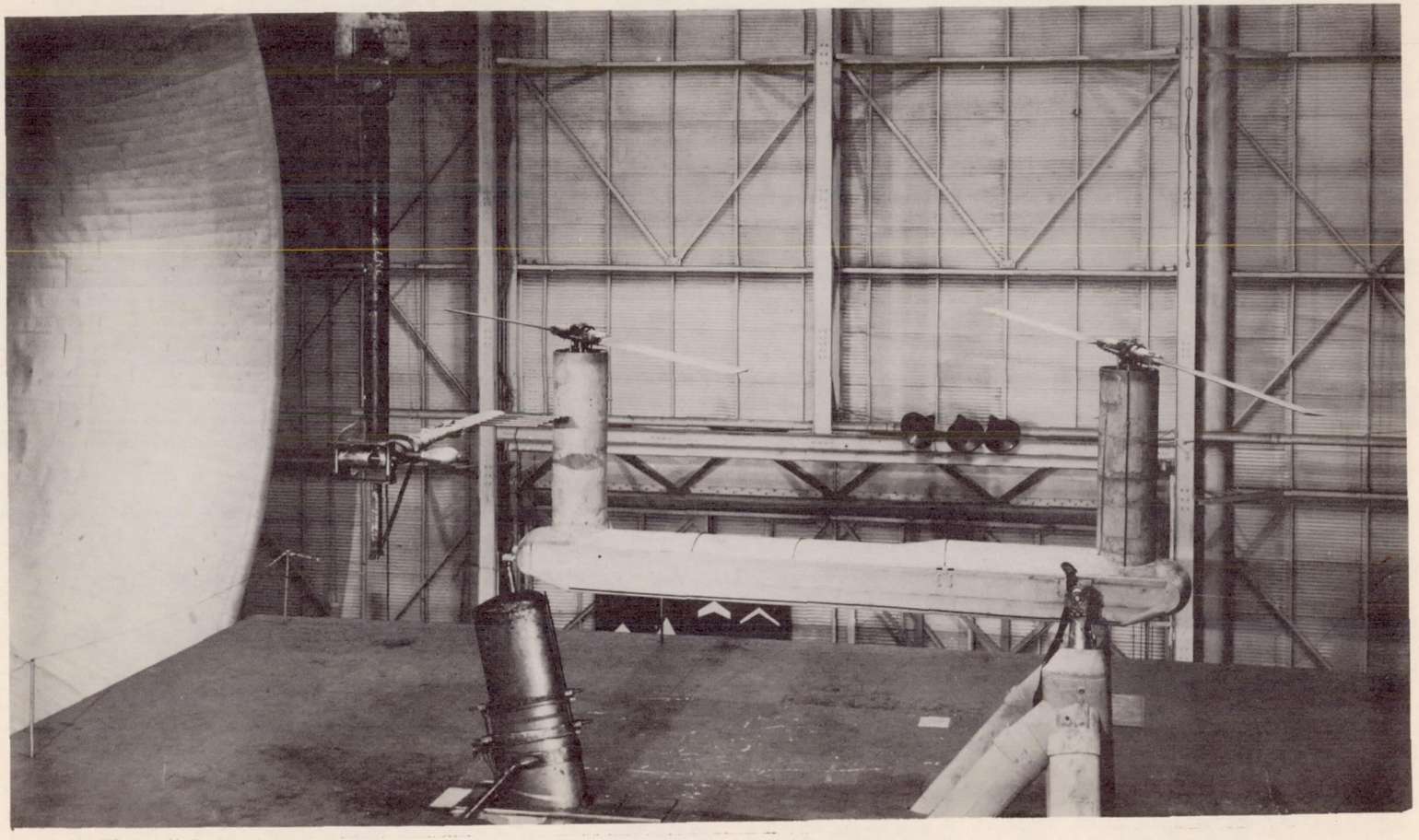

L-79081

Figure 2.-Tandem-rotor apparatus mounted in the Langley full-scale tunnel.

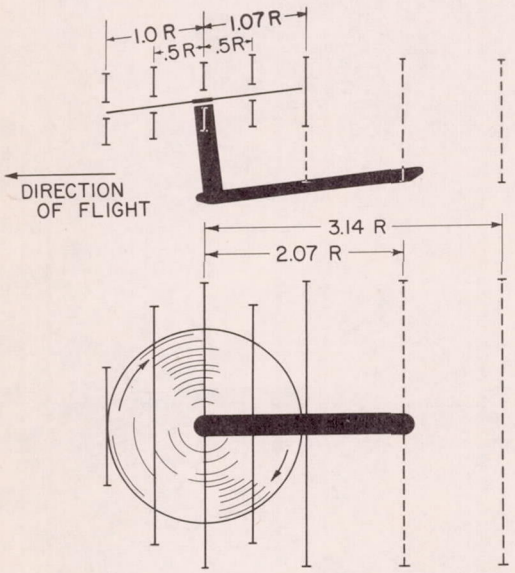

Figure 3.- Survey planes used in single-rotor tests.

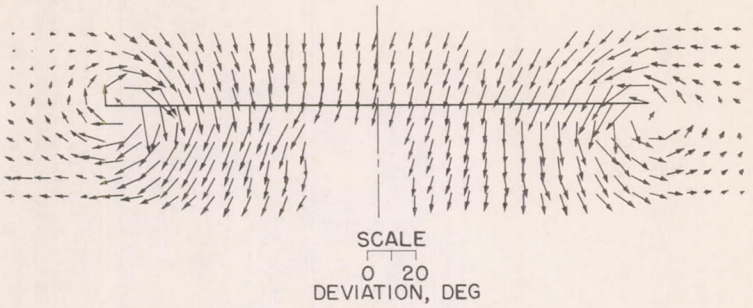

(a) Stream angles 7 percent of a radius behind trailing edge of single rotor.

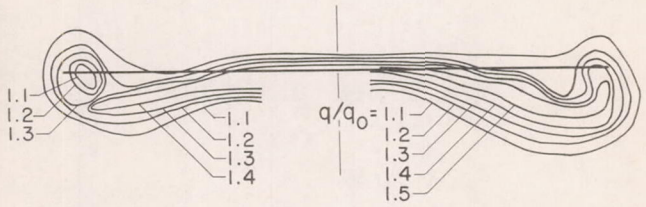

(b) Variation of local dynamic pressure q/q_o at 7 percent of a radius behind trailing edge of single rotor.

Figure 4.- Flow behind trailing edge of single rotor. $\mu = 0.15$; $C_L = 0.321$.

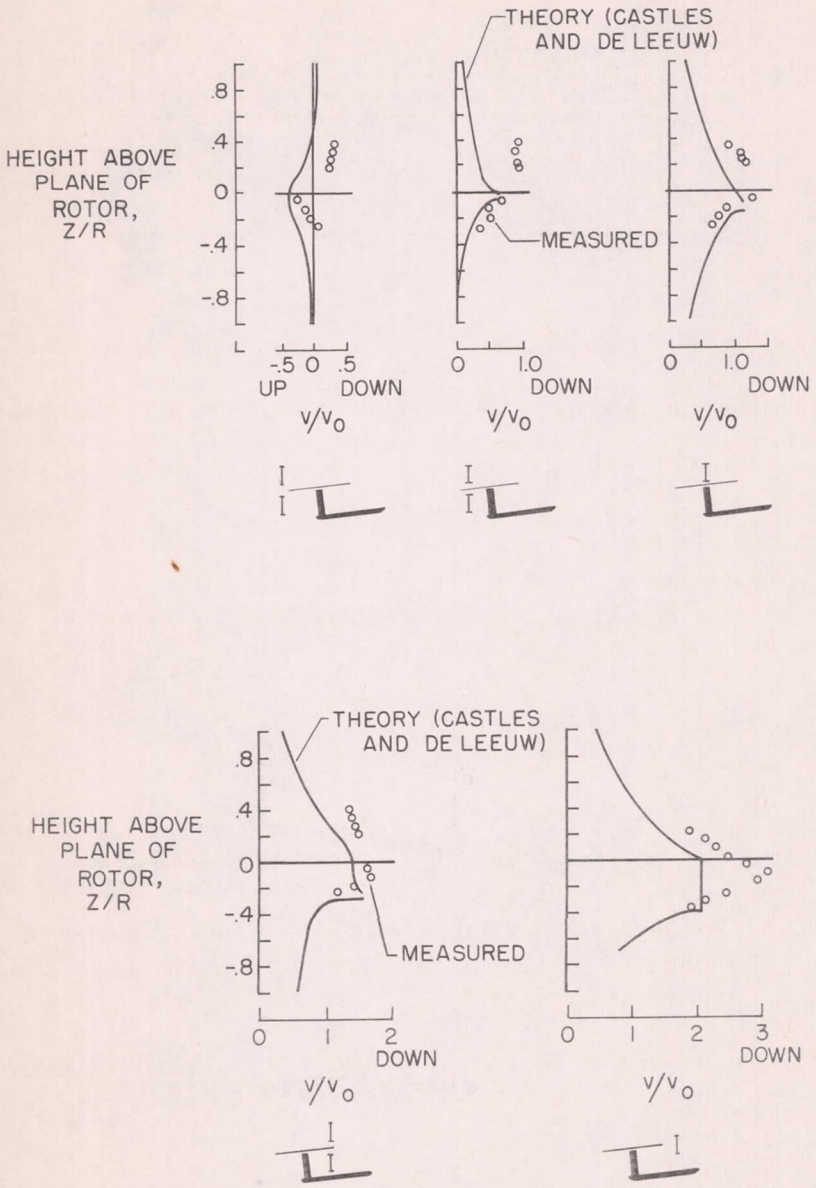

Figure 5.- Variation of induced velocity near single rotor. $\mu = 0.15$; $C_L = 0.321$; $\chi = 82.7^{\circ}$.

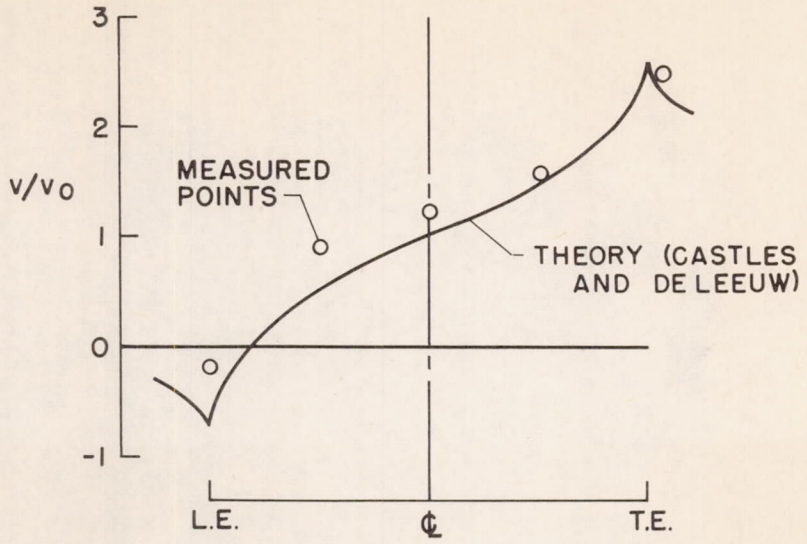

Figure 6.- Variation of induced velocity in plane of rotor.

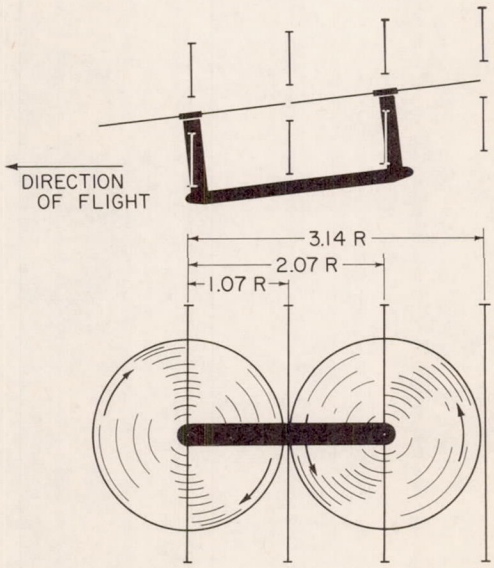

Figure 7.- Survey planes used in tandem-rotor tests.

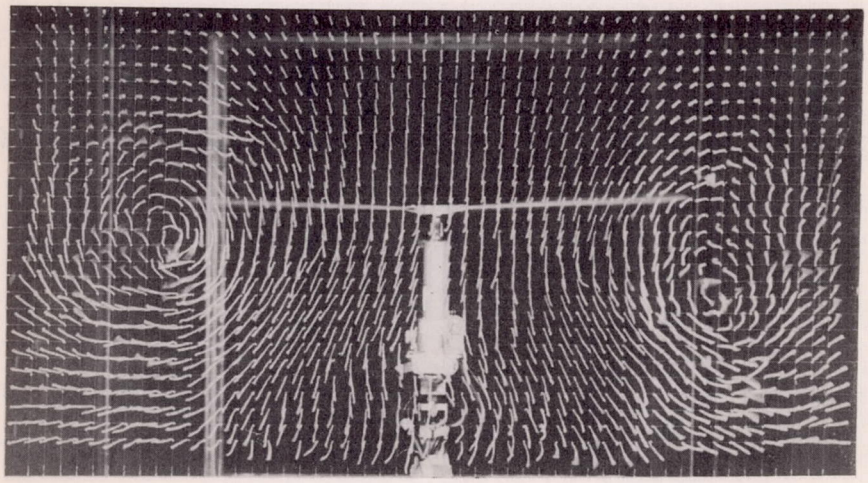

Figure 8.- Tuft-grid photograph of flow behind tandem-rotor helicopter in the Langley stability tunnel.

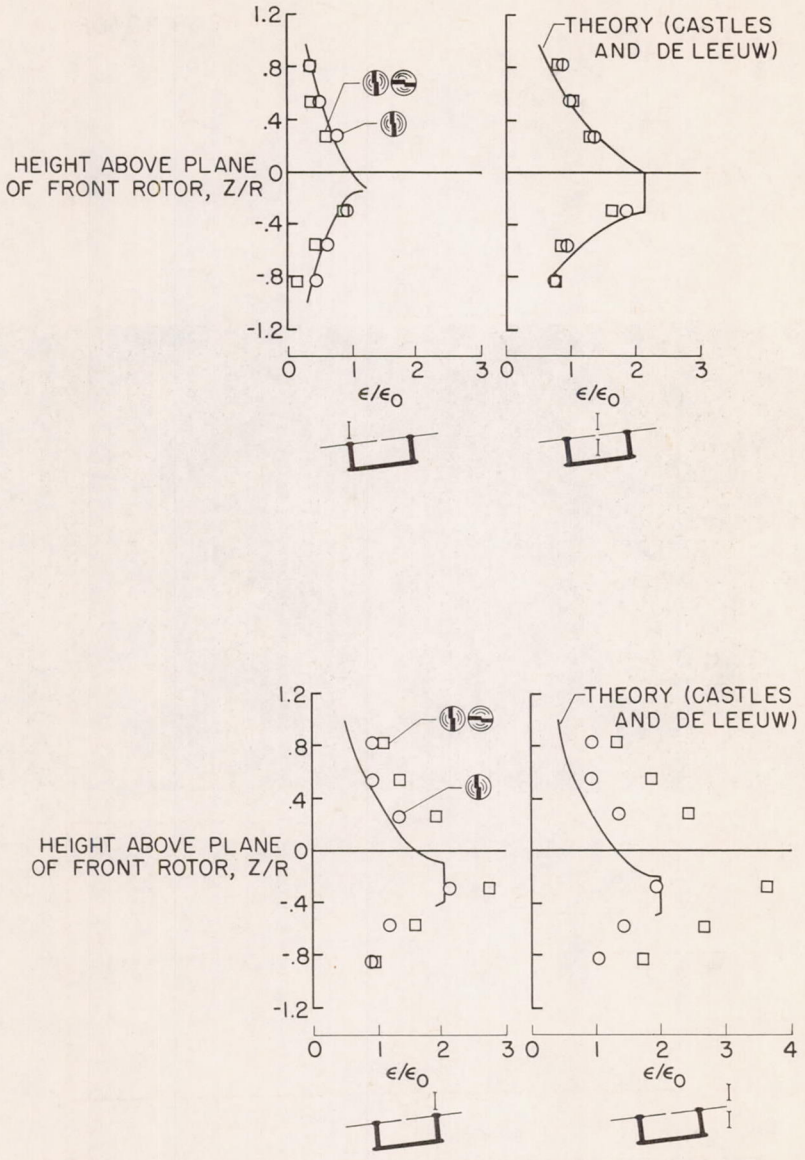

Figure 9.- Variation of downwash near single and tandem rotors. $\mu = 0.15$; $C_L = 0.302$; $\chi = 83.4^\circ$.

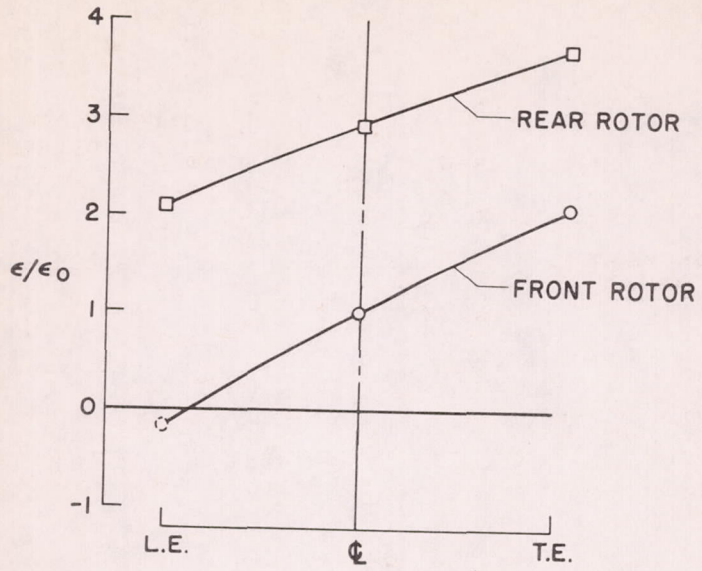

Figure 10.- Comparison of downwash in plane of front and rear rotors of tandem-rotor helicopter.

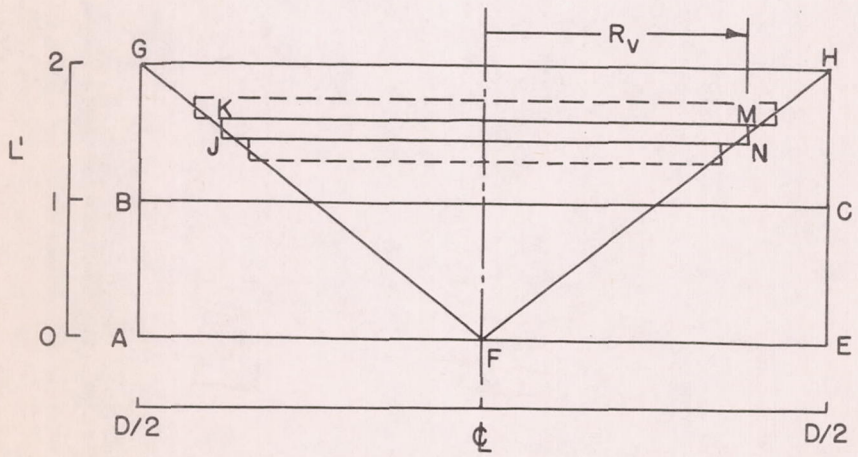

Figure 11.- Radial loading on diameter of rotor of appendix A.